Smart Structures and Systems, *Vol. 32, No. 1 (2023) 9-21*
https://doi.org/10.12989/sss.2023.32.1.009

A novel adaptive unscented Kalman Filter with forgetting factor for the identification of the time-variant structural parameters

Yanzhe Zhang [1,2§], Yong Ding [3,4§], Jianqing Bu*[1,5,6] and Lina Guo [7]

[1] *State Key Laboratory of Mechanical Behavior and System Safety of Traffic Engineering Structures, Shijiazhuang Tiedao University, Shijiazhuang 050043, China*
[2] *School of Civil Engineering, Shijiazhuang Tiedao University, Shijiazhuang 050043, China*
[3] *School of Civil Engineering, Harbin Institute of Technology, Harbin 150090, China*
[4] *Key Lab of Structures Dynamic Behavior and Control (Harbin Institute of Technology), Ministry of Education, Heilongjiang, Harbin 150090, China*
[5] *School of Traffic and Transportation, Shijiazhuang Tiedao University, Shijiazhuang 050043, China*
[6] *Key Laboratory of traffic safety and control of Hebei Province, China*
[7] *College of Water Conservancy and Civil Engineering, Northeast Agricultural University, Harbin 150048, China*

(*Received June 9, 2022, Revised December 30, 2022, Accepted May 31, 2023*)

Abstract. The parameters of civil engineering structures have time-variant characteristics during their service. When extremely large external excitations, such as earthquake excitation to buildings or overweight vehicles to bridges, apply to structures, sudden or gradual damage may be caused. It is crucially necessary to detect the occurrence time and severity of the damage. The unscented Kalman filter (UKF), as one efficient estimator, is usually used to conduct the recursive identification of parameters. However, the conventional UKF algorithm has a weak tracking ability for time-variant structural parameters. To improve the identification ability of time-variant parameters, an adaptive UKF with forgetting factor (AUKF-FF) algorithm, in which the state covariance, innovation covariance and cross covariance are updated simultaneously with the help of the forgetting factor, is proposed. To verify the effectiveness of the method, this paper conducted two case studies as follows: the identification of time-variant parameters of a simply supported bridge when the vehicle passing, and the model updating of a six-story concrete frame structure with field test during the Yangbi earthquake excitation in Yunnan Province, China. The comparison results of the numerical studies show that the proposed method is superior to the conventional UKF algorithm for the time-variant parameter identification in convergence speed, accuracy and adaptability to the sampling frequency. The field test studies demonstrate that the proposed method can provide suggestions for solving practical problems.

Keywords: adaptive tracking; forgetting factor; model updating; state variable; time-variant parameters

1. Introduction

Civil engineering structures will bear various loads during their service, such as pedestrians, vehicles, wind, earthquakes, dead load and other environmental excitation, in which dynamic load excitation has a greater destructive effect on structures (Doebling *et al*. 1998). When a structure is subjected to an extremely large dynamic load, structural damage may be caused, which can be related to sudden or gradual changes in structural parameters. Tracking the time-variant characteristics of structural parameters plays a great role in decision-making and cost reduction for structural maintenance. In the structural evaluation after the extremely large excitation, the time-variant parameters identification is still a challenging job, especially for strongly nonlinear structures (Rahimi *et al*. 2017).

At present, structural parameter identification methods are mainly divided into two categories: data-driven (Taffese and Sistonen 2017) and model-driven (Yan *et al*. 2016). Generally, data-driven methods, such as regression algorithms, classification algorithms and clustering algorithms (Yan *et al*. 2016), do not need to know the structural model information in advance. They only need data analysis to determine structural parameters. For example, in the civil engineering industry, many scholars have used various data-driven methods to identify the mass, stiffness, strength, surface roughness and long-term deformation parameters (Soyoz and Feng 2009, Nguyen *et al*. 2021, Mulay *et al*. 2019, Shu *et al*. 2021), which are all time-invariant. To solve the time-variant parameter identification problem, Ahmed-Ali *et al*. (2009) proposed a sliding-neural network observer based on the radial basis function network to identify the time-varying parameters of nonlinear systems and validated the network through a numerical model. However, it is not applied to practical structures. In other areas, such as the economic market (Chen and Zhou 2020), lithium-ion batteries (Masti *et al*. 2021), diesel/compression ignition engines (Chin *et al*. 2020, Bao *et al*. 2020) and induction motors (Cui *et al*. 2019), time-variant parameters or parameter-varying

*Corresponding author, Ph.D., Professor,
E-mail: bujq@stdu.edu.cn
§ The first two authors, Yanzhe Zhang and Yong Ding, contributed equally to this research work.

ISSN: 1738-1584 (Print), 1738-1991 (Online)

problems based on data-driven algorithms are considered. However, only Chen and Zhou (2020) and Bao *et al*. (2020) considered the problem of time-varying parameter identification.

As can be concluded from the above research, only a small part of the literature uses the corresponding data-driven method to solve the time-variant parameter identification problem because most of the state-of-the-art machine learning methods in the literature focus on the data classification problems until now (Chen and Zhou 2020). Besides, to get a relatively accurate data-driven model, it usually needs a large number of measurement responses as inputs to train the data model, and the training time consumption is usually huge, especially for the more complex and larger civil engineering structures.

To identify the structural parameters with fewer measurement data and time, various model-driven methods, such as the least squares estimation (LSE), Kalman filter (KF), extended Kalman filter (EKF), unscented Kalman filter (UKF), Monte Carlo filter (MCF), Iteration Regularization and other methods (Doebling *et al*. 1998, Yang and Lin 2005, Yang *et al*. 2006, Pappalardo and Guida 2016, Chung and Sato 2006, Pappalardo and Guida 2017, Humar *et al*. 2006, Manoach *et al*. 2012, Wang *et al*. 2018), are proposed. These methods directly use optimization algorithms to identify structural parameters based on the equation of motion or equations in state space. Among them, the LSE is originally an offline identification method and suitable for linear structures. It has low operation efficiency and applicability because executing it requires knowing the whole structural response. Although the modified recursive LSE method is proposed afterward for online identification, its ability to identify the time-variant parameters needs to be improved. The MCF can be applied to the nonlinear system, but its calculation needs to generate a large number of sampling points, which is also inefficient (Calabrese *et al*. 2018). Compared with LSE and MCF, the KF belongs to a fast online identification method with recursive characteristics. When the new data information is collected, it can update the identification results through Bayesian data fusion technology (Cao *et al*. 2020, Naranjo-Pérez *et al*. 2020). As an extension of KF, the UKF does not need to solve the complex Jacobian matrix like EKF, approximates the probability density distribution of nonlinear function through the deterministic sampling by unscented transformation (UT) without introducing excessive error caused by the linearization of a complex nonlinear function, and has second-order accuracy, even third-order accuracy for Gaussian random variables (Naranjo-Pérez *et al*. 2020), which has been widely concerned and applied in recent years. For example, many scholars have applied UKF to the identification of hysteretic model parameters (Cao *et al*. 2020), nonlinear structural finite element model updating (Astroza *et al*. 2019a), dynamic load estimation (Guo *et al*. 2018) and the synchronous identification of parameters and loads (Ding *et al*. 2017). Unfortunately, the above researches do not consider the time-variant characteristics in the identification process either.

To overcome the inefficiency of conventional UKF in identifying time-variant parameters or systems (Calabrese *et al*. 2018, Bisht and Singh 2014), various adaptive algorithms have been proposed. According to the correction principle, these adaptive algorithms are mainly divided into two categories: state covariance correction methods (Bisht and Singh 2014, Xiao *et al*. 2020, Schleiter and Altay 2020) and noise parameter correction methods (Calabrese *et al*. 2018, Zhou *et al*. 2019, Wang *et al*. 2019, Astroza *et al*. 2019b, Song *et al*. 2020, Asl *et al*. 2019, Hu *et al*. 2021, Sadhukhan *et al*. 2021). As the sensing technology becomes more and more advanced, the influence of measurement noise interference will be smaller and smaller. Meanwhile, the error caused by model uncertainty will be highlighted. Because the model uncertainty is closely related to the state covariance, how to modify the covariance matrix more conveniently without adding additional program cycles is closely related to the accuracy, practicability and computational efficiency of the algorithm. Besides, after verification, the above-mentioned adaptive methods based on the state covariance correction technique are all suitable for identifying time-variant parameters, while only Wang *et al*. (2019) and Asl *et al*. (2019) truly considered the identification of time-variant parameters with the help of noise parameter correction technique. Therefore, this paper achieves the purpose of automatically tracking and identifying time-variant parameters based on the state covariance correction method. Different from the above-mentioned adaptive methods, this paper introduces a forgetting factor to modify the state covariance, innovation covariance and cross covariance at the same time, to expand the role of new measurement and weaken the cumulative error of previous data. Furthermore, there is no additional 'for loop' in the program. By this means, the proposed method can consider the updating of multiple time-variant parameters in the state vector at the same time without extra iteration and adding extra time consumption.

The specific arrangement of this article is as follows. Section II is the introduction of algorithm modification, which mainly describes the conventional UKF algorithm, the modified adaptive UKF with forgetting factor (AUKF-FF) algorithm and a simple comparison between UKF and AUKF-FF. Section III is the numerical studies validation, which uses the vehicle bridge system (VBS) to verify the effectiveness of the proposed method. Section VI is the field test validation, in which a real six-story frame structure subjected to Yangbi earthquake is investigated. Finally, section V is the conclusion.

2. Algorithm modification and comparison

2.1 The UKF Algorithm

Assume there exists a nonlinear system in which the state prediction equation and observation equation in discrete-time form can be expressed as Eqs. (1)~(2) respectively.

$$X_k = f(X_{k-1}, U_{k-1}) + w_{k\text{-}1} \tag{1}$$

$$Y_k = h(X_k) + v_k \tag{2}$$

where k is the discrete time, **X** represents the system state vector, **U** represents the system input matrix, **Y** represents the system observation vector, $f(\cdot)$ and $h(\cdot)$ denote the nonlinear function, **w** and **v** are process noise and observation noise with the mean value of zero and covariance of **Q** and **R**, respectively.

The initial parameters of the UKF algorithm are $\hat{X}_0^+ = E(X_0)$ and $\hat{P}_0^+ = E[(X_0 - \hat{X}_0^+)(X_0 - \hat{X}_0^+)^T]$, where $\hat{X}_0^+$ represents the initial state vector and $\mathbf{X}_0$ denotes the initial values determined by experience, finite element analysis or design drawings; $\hat{P}_0^+$ is the initial state covariance matrix and is composed of uncorrelated diagonal elements (Mariani and Ghisi 2007). $\hat{P}_0^+$represents the confidence in the initial state estimates and must be specified a prior. In the absence of any prior knowledge of the $\mathbf{X}_0$, it is common to assume high values for the $\hat{P}_0^+$ (Jategaonkar and Plaetenschke 1988, Chowdhary and Jategaonkar 2010).

Then $(2n + 1)$ sigma points need to be produced by UT, such as Eq. (3).

$$\hat{\chi}_{k-1} = \left[\hat{X}_{k\text{-}1}^+, \hat{X}_{k\text{-}1}^+ + \sqrt{n+\lambda}\left(\sqrt{P_{k-1}^+}\right)_i, \hat{X}_{k\text{-}1}^+ - \sqrt{n+\lambda}\left(\sqrt{P_{k-1}^+}\right)_i\right] \tag{3}$$

where i = 1, 2, ..., n and n is equal to the number of variables in the state vector, λ is the gain parameter related to the dimension and distribution of the state vector (Julier *et al*. 1995). To ensure the symmetry and positive characterization of the covariance, the singular value decomposition method proposed by Guo *et al*. (2018) is used to calculate the square root of state covariance. Then the a priori estimation of each sigma point is solved by Eq. (4) based on the state prediction equation.

$$\hat{\chi}_k^{(i)} = f\left(\hat{\chi}_{k-1}^{(i)},\ U_{k-1}\right) \tag{4}$$

The expectation and state covariance of a priori estimation are calculated as Eqs. (5) to (8).

$$\hat{\chi}_k^- = \sum_{i=0}^{2n} W_m^i\, \hat{\chi}_k^{(i)} \tag{5}$$

$$P_k^- = \sum_{i=0}^{2n} W_c^i\left(\hat{\chi}_k^{(i)} - \hat{\chi}_k^-\right)\left(\hat{\chi}_k^{(i)} - \hat{\chi}_k^-\right)^T + Q_k \tag{6}$$

$$W_c^i = \begin{cases} \dfrac{\lambda}{n+\lambda} + 1 - a^2 + b, & i = 0 \\ \dfrac{1}{2(n+\lambda)}, & i = 1, 2, \cdots, 2n \end{cases} \tag{7}$$

$$W_m^i = \begin{cases} \dfrac{\lambda}{n+\lambda}, & i = 0 \\ \dfrac{1}{2(n+\lambda)}, & i = 1, 2, \cdots, 2n \end{cases} \tag{8}$$

where a is the mean adjustment coefficient, and $10^{-4} \le a \le 1$; b is the variance adjustment coefficient, generally taking $b = 2$.

Generate $(2n + 1)$ sigma points $\hat{\chi}_k^{<i>}$ again based on the $\hat{\chi}_k^-$ and P_k^- calculated by Eqs. (5) and (6). According to the observation equation, the process of the Kth updating is as follows

$$\hat{y}_k^{(i)} = h(\hat{\chi}_k^{<i>}) \tag{9}$$

$$\hat{y}_k = \sum_{i=0}^{2n} W_m^i\, \hat{y}_k^{(i)} \tag{10}$$

$$P_{yy,k} = \sum_{i=0}^{2n} W_c^i\left(\hat{y}_k^{(i)} - \hat{y}_k\right)\left(\hat{y}_k^{(i)} - \hat{y}_k\right)^T + R_k \tag{11}$$

$$P_{xy,k} = \sum_{i=0}^{2n} W_c^i\left(\hat{\chi}_k^{(i)} - \hat{\chi}_k^-\right)\left(\hat{y}_k^{(i)} - \hat{y}_k\right)^T \tag{12}$$

$$K_k = P_{xy,k} P_{yy,k}^{-1} \tag{13}$$

$$\hat{\chi}_k^+ = \hat{\chi}_k^- + K_k(y_k - \hat{y}_k) \tag{14}$$

$$P_k^+ = P_k^- - K_k P_{\mathrm{yy},k} K_k^T \tag{15}$$

where $\mathbf{K}_k$ is the Kalman gain matrix, $\mathbf{P}_{yy,k}$ is the innovation covariance at step k, $\mathbf{P}_{xy,k}$ is the cross covariance of step k, $\hat{\chi}_k^+$ is the Kth-step posteriori estimation corrected by the measurement data. The above Eqs. (1) to (14) represent a one-time-step UKF recursive process.

2.2 The adaptive UKF with forgetting factor

In the recursive process of UKF, because the weight values of UT in each step are the same, the data in each step has the same effect on filtering. As the old data accumulates, its influence on the update of the state vector gradually increases. Meanwhile, the update effect of new data gradually decreases, so that the filtering process tends to be stable (refer to Fig. 2(f)). Thus, when the parameter changes at some time, if there are no corrective measures, the new measurement data cannot update the state estimation in time, leading to the failure of tracking time-variant parameters.

To strengthen the ability of UKF to identify time-variant parameters. Firstly, refer to the method proposed by Bisht and Singh (2014), this paper also selects ε and $\mathbf{P}_{yy}$ to construct a sensitive parameter η that can predict the change time of parameters, and the discrete form is as shown in Eq. (16).

$$\eta_k = \varepsilon_k^T (\boldsymbol{P}_{yy,k})^{-1} \varepsilon_k \tag{16}$$

Where ε_k is the Kth-step estimation error, and $\varepsilon_k = y_k - \hat{y}_k$.

Secondly, to intelligently call the adaptive algorithm, it is necessary to define a decision threshold value η_0. Bisht and Singh (2014) proposed that η_0 is a constant and obeys the Chi-square distribution with the same number of degrees of freedom as that in observed values. By specifying a transcendental probability P = 0.001, the

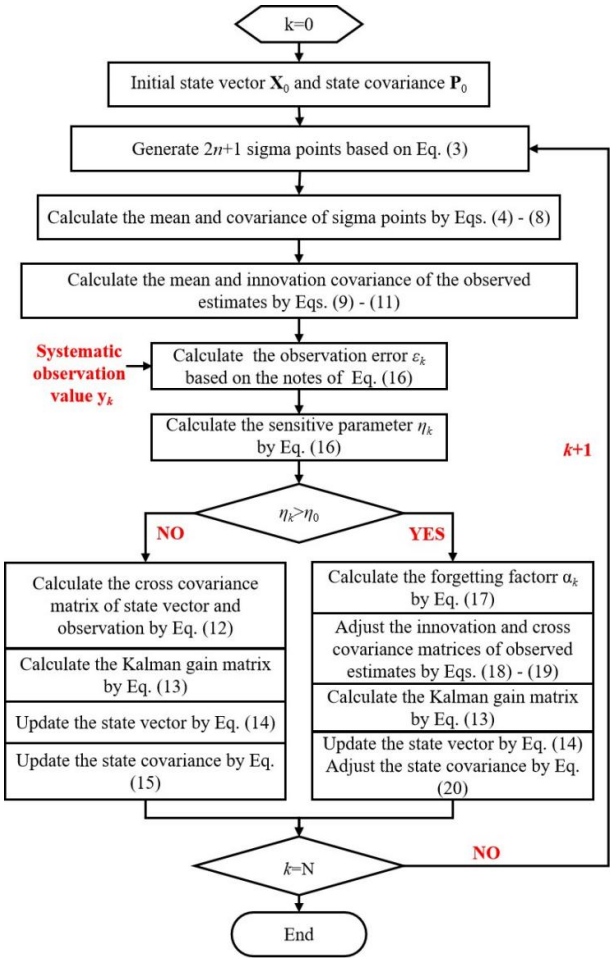

Fig. 1 Algorithm flow of AUKF-FF

threshold value η_0 can be obtained through the Chi-square inverse cumulative distribution function. However, in practice, there are two disadvantages (Rahimi *et al*. 2017): (1) it requires the prior information of all data due to η_0 determined based on the statistical characteristics, and (2) if the predefined value is unreasonable, it may lead to divergent or erroneous results. After practical verification, it is found that the η_0 calculated by Bisht and Singh (2014) can ensure good results on the condition that the noise is small and η calculated by Eq. (16) has obvious variation characteristics. Whereas, when the noise is large, continuing to use a fixed η_0 will lead to a convergence problem.

To adapt to different noise levels, this paper proposes a more reasonable and simple threshold determination method. It mainly consists of the following three steps: (1) calculate the time history curve of η by UKF; (2) find the maximum value η_t (refer to Fig. 2(d)) before the curve mutating; (3) take the number slightly larger than η_t as η_0 (refer to Fig. 2(d)) and then fine tunes. Attention, if the time history curve of η is stable and it is hard to judge the location where the change occurs, it shows two situations: (1) the parameters may not change during the identification process; (2) the noise interference is too large to identify the real curve features. Generally, it can be obviously seen where the curve mutation is by the eyes if the parameters indeed change with time and the noise level is reasonable.

Thirdly, we need to define a forgetting factor α, as shown in Eq. (17), to modify covariance once some $\eta_k > \eta_0$, where $\alpha_k \in (0,1)$. The essence of α is to enlarge the state covariance and Kalman gain matrix, highlight the role of new measurements, and improve the tracking ability of the algorithm.

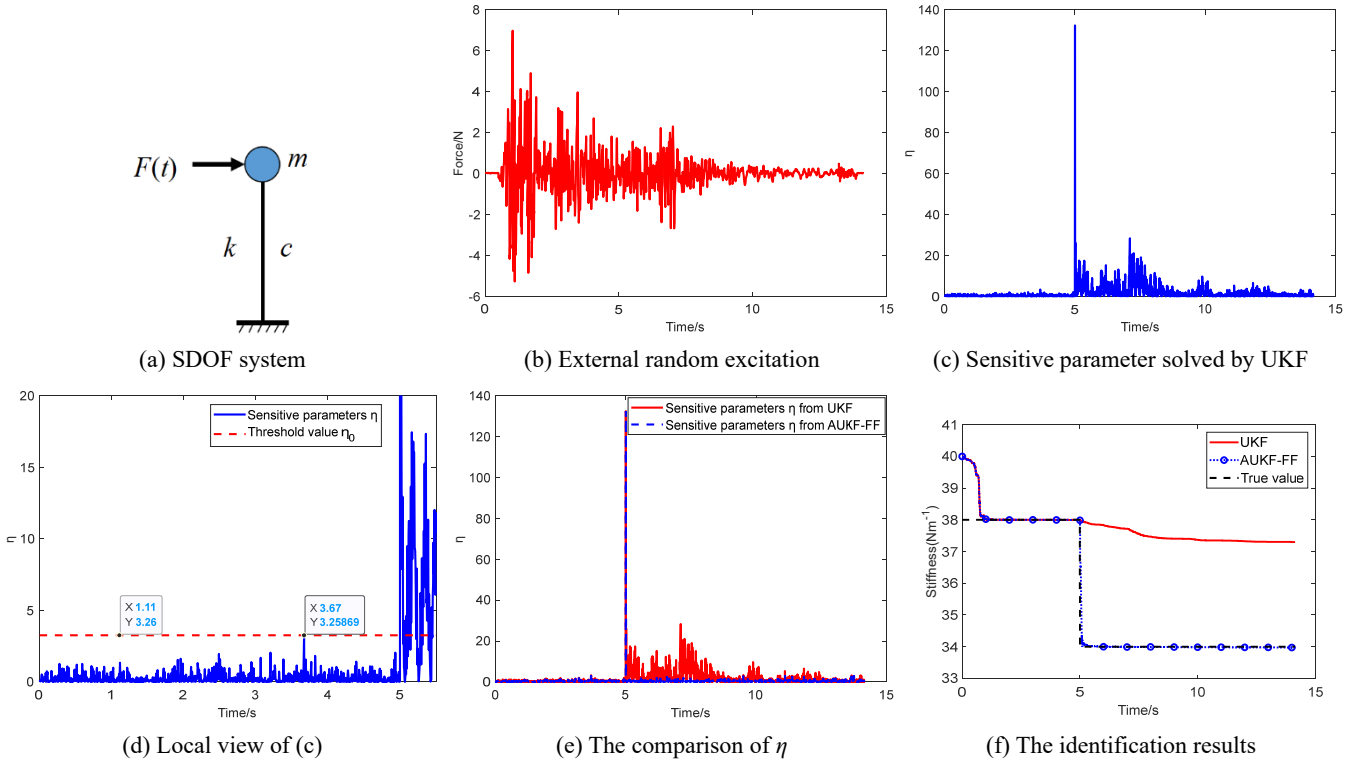

(a) SDOF system (b) External random excitation (c) Sensitive parameter solved by UKF

(d) Local view of (c) (e) The comparison of η (f) The identification results

Fig. 2 The effect of adaptive UKF with forgetting factor

$$\alpha_k = \begin{cases} 1, & tr(\varepsilon_k \varepsilon_k^T) \le tr(P_{yy,k}) \\ \dfrac{tr(P_{yy,k})}{tr(\varepsilon_k \varepsilon_k^T)}, & tr(\varepsilon_k \varepsilon_k^T) \ge tr(P_{yy,k}) \end{cases} \tag{17}$$

Finally, with the forgetting factor, the novel covariance updating method is as formulas (18)~(20). And please see Fig. 1 for a specific flow chart.

$$\hat{P}_{yy,k} = \frac{1}{\alpha_k} \sum_{i=0}^{2n} W_c^i \left(\hat{y}_k^{(i)} - \hat{y}_k\right) \left(\hat{y}_k^{(i)} - \hat{y}_k\right)^T + R_k \tag{18}$$

$$P_{xy,k} = \frac{1}{\alpha_k} \sum_{i=0}^{2n} W_c^i \left(\hat{x}_k^{(i)} - \hat{x}_k^-\right) \left(\hat{y}_k^{(i)} - \hat{y}_k\right)^T \tag{19}$$

$$P_k^+ = \frac{1}{\alpha_k} P_k^- - K_k P_{yy,k} K_k^T \tag{20}$$

2.3 Comparison study

To better illustrate the effect of AUKF-FF, here considers a single degree of freedom (SDOF) system, as shown in Fig. 2. The control equation of the SDOF system can be written as Eq. (21).

$$m\ddot{u}(t) + c\dot{u}(t) + ku(t) = F(t) \tag{21}$$

where m, c and k are the mass, damping and stiffness of the SDOF system, respectively; u, $\dot{u}$ and $\ddot{u}$ represent the displacement, velocity and acceleration, respectively; F stands for the external excitation.

Assume the mass and damping are constant, such as taking m = 0.1 kg and c = 0.32 Nsm^{-1}. Meanwhile, assume the stiffness is time-variant and the specific change process is as follows. Under the excitation of Fig. 2(b), in the first 5 seconds, take k = 38 Nm^{-1}, and in the fifth second, let k = 34 Nm^{-1} abruptly. Firstly, the acceleration$\ddot{u}$can be solved as a forward problem based on the fourth order Runge-Kutta method. Then as an inverse problem, the calculated acceleration is taken as the observed value to identify the stiffness of the SDOF system. Here $\mathbf{X}_0$ is made up of initial displacement, initial velocity and initial stiffness. Let $\mathbf{X}_0$ = $[0, 0, 40]^T$ and $\mathbf{P}_0$ = $diag(10^{-8}, 10^{-8}, 1)$. At the same time, the process noise covariance and measurement noise covariance matrices take $1 \times 10^{-8}\mathbf{I}$ respectively. The specific filtering results are shown in Fig. 2(f).

From Fig. 2(c), we can find the instant when the stiffness parameter change occurs. Besides, the maximum η before the stiffness changing is about 3.25869 (the blue curve in Fig. 2(d)). Therefore, we can first take η_0 = 3.26 (the red dash curve in Fig. 2(d)). As can be seen from Fig. 2(e), η is very small before the stiffness changes, no matter what the filtering algorithm is. This phenomenon shows that the parameter keeps time-invariant. Continuing to observe Fig. 2(e), we can find η is relatively larger than before after the stiffness changing based on UKF. The large η means a big identification error which can lead to wrong results (Fig. 2(f)). However, the proposed AUKF-FF algorithm can solve the above problem well. After the 5th second, the sensitive parameter η is again decreased to very small values with the help of AUKF-FF (Fig. 2(e)). And the identified value is in good agreement with the real value based on the AUKF-FF method (Fig. 2(f)).

3. Numerical simulation studies of adaptive UKF with forgetting factor

3.1 Vehicle-bridge-system

To further explain the effectiveness of the proposed method, this section selects a simply supported bridge to identify its time-variant stiffness parameters based on the vehicle bridge interaction force when the vehicle crosses the bridge, in which the bridge section is constant, as shown in Fig. 3. The specific parameters are: bridge span L = 21 m, cross-sectional area A = 1.2 m^2, section moment of inertia I = 0.12 m^4, elastic modulus E = 2.4 × 10^{10} Nm^{-2} and density ρ = 2000 kgm^{-3}.

In this paper, the finite element model (FEM) of the bridge is established by the Euler Bernoulli beam element. Considering the calculation efficiency and accuracy, the bridge is divided into six elements. Because each element has 2 nodes and each node has 2 degrees of freedom, the total degree of freedom of the bridge is 14. Besides, to simulate real road conditions, the surface roughness is considered and characterized by random numbers obeying normal distribution. The motion control differential equation of the bridge is obtained based on D'Alembert's principle, as shown in Eq. (22).

$$M_b\ddot{u}_b(t) + C_b\dot{u}_b(t) + K_b u_b(t) = LF(t) \tag{22}$$

where $\mathbf{M}_b$, $\mathbf{K}_b$ and $\mathbf{C}_b$ represent the mass, stiffness and damping matrices of the bridge, respectively; Rayleigh damping type is adopted and the damping ratio is taken as 0.015; $\mathbf{u}_b$ represents the displacement and the overdots represent the time derivative; $\mathbf{L}$ stands for the position vector, such as $\mathbf{L}$ = {0, 0, …, $L_i(t)$,…, 0, 0} in which $L_i(t)$ is

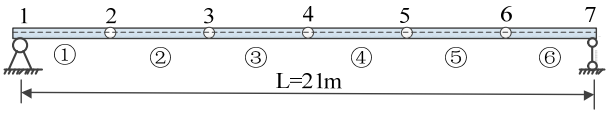

Fig. 3 The FEM of the simply supported bridge

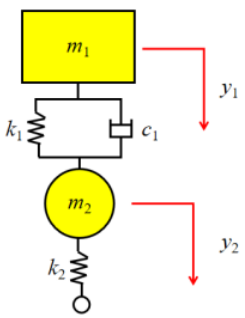

Fig. 4 The vehicle model

a Hermitian function and $L_i(t) = [1 - 3\xi^2 + 2\xi^3,\ l\xi(1-\xi)^2,\ \xi^2(3-2\xi),\ -l\xi^2(1-\xi)]$, where $\xi = x/l$, x is the distance the vehicle moves on one element and l is the element length; **F** is the load.

The vehicle system model has two degrees of freedom (Fig. 4) and the system parameters include the body mass $m_1 = 3.6 \times 10^4$ kg, bogie mass $m_2 = 2.5 \times 10^2$ kg, secondary suspension stiffness $k_1 = 6.0 \times 10^5$ Nm^{-1}, secondary suspension damping $c = 1.0 \times 10^3$ Nsm^{-1} and primary suspension stiffness $k_2 = 8.5 \times 10^5$ Nm^{-1}. The moving speed is set to 8.4 ms^{-1}. Besides, assume there is no other external excitation. The vehicle motion equation is shown in Eq. (23).

$$\begin{cases} m_1\ddot{u}_1 + c(\dot{u}_1 - \dot{u}_2) + k_1(u_1 - u_2) = 0 \\ m_2\ddot{u}_2 + c(\dot{u}_2 - \dot{u}_1) + k_1(u_2 - u_1) + k_2(u_2 - u(x(t)) - r(x(t))) = 0 \end{cases} \tag{23}$$

where u, $\dot{u}$ and $\ddot{u}$ represent the vertical displacement, velocity and acceleration of the vehicle body or bogie respectively, among which subscript 1 represents the vehicle body and subscript 2 represents the bogie; $u(x(t))$ represents the vertical displacement of the bridge at position $x(t)$; $r(x(t))$ represents the roughness of the bridge at position $x(t)$; $x(t)$ is the position of the vehicle at time t.

The formula of vehicle bridge interaction force is deduced as Eq. (24).

$$\begin{aligned} &F_{int}(t) \\ &= (m_1 + m_2)g + k_2\left(u_2 - u\big(x(t)\big)r\big(x(t)\big)\right) \\ &= (m_1 + m_2)g - m_1\ddot{u}_1 - m_2\ddot{u}_2 \end{aligned} \tag{24}$$

Through Eq. (24), the vehicle bridge interaction force is closely related to the mass and acceleration of the vehicle body and bogie, which provides relevant ideas and methods for practical measurement. Based on the coupling relationship between contact force and displacement, the motion control equation of the vehicle bridge system is established, as shown in Eq. (25).

$$\boldsymbol{M}\ddot{\boldsymbol{U}}(\boldsymbol{t}) + \boldsymbol{C}\dot{\boldsymbol{U}}(\boldsymbol{t}) + \boldsymbol{K}\boldsymbol{U}(\boldsymbol{t}) = \boldsymbol{F}(\boldsymbol{t}) \tag{25}$$

Where

$$\boldsymbol{M} = \begin{bmatrix} \boldsymbol{M}_b & L^T m_1 & L^T m_2 \\ 0 & m_1 & 0 \\ 0 & 0 & m_2 \end{bmatrix}, \quad \boldsymbol{C} = \begin{bmatrix} \boldsymbol{C}_b & 0 & 0 \\ 0 & c & -c \\ 0 & -c & c \end{bmatrix},$$

$$U(t) = \begin{bmatrix} u_b(t) \\ u_1(t) \\ u_2(t) \end{bmatrix}$$

$$\boldsymbol{K} = \begin{bmatrix} \boldsymbol{K}_b & 0 & 0 \\ 0 & k_1 & -k_1 \\ -k_2 L & -k_1 & k_1 + k_2 \end{bmatrix}, \quad \boldsymbol{F} = \begin{bmatrix} L^T[(m_1 + m_2)g] \\ 0 \\ k_2 r\big(x(t)\big) \end{bmatrix}$$

The above **M**, **C** and **K** denote the mass, stiffness and damping matrices of the VBS, respectively; **U**, $\dot{\boldsymbol{U}}$ and $\ddot{\boldsymbol{U}}$ represent the displacement, velocity and acceleration responses, respectively; **F** stands for the excitation. Other symbols are consistent with the above.

3.2 Bridge time-variant parameters identification

The main mechanical function of the simply supported bridge is bending resistance. When the bridge section form, materials and reinforcement are determined, the parameter affecting its bending stiffness is mainly the elastic modulus. Therefore, the elastic modulus E is taken as the parameter to be identified in this part.

After trial and error, it is found that synchronously identifying all the elastic modulus (E_1~E_6) of the bridge (Fig. 3) is hard. From a mathematical point of view, the reason may be that the beams ① and ⑥ in Fig. 3 are not sensitive to the same observation values. To explain the reason, a brief analysis is given here. In the analysis, we use the same observation values to identify each beam element respectively by UKF. This means that a total of six parallel simulation experiments are set up. Each test assumes that only one beam element is unknown, and the time-variant characteristics of the unknown beam element are the same. Considering the convenience of practical measurement and the high accuracy of multiple measurement points, here takes the five vertical displacements of nodes 2 ~ 6 in Fig. 3 as the observation values. Other settings remain the same for

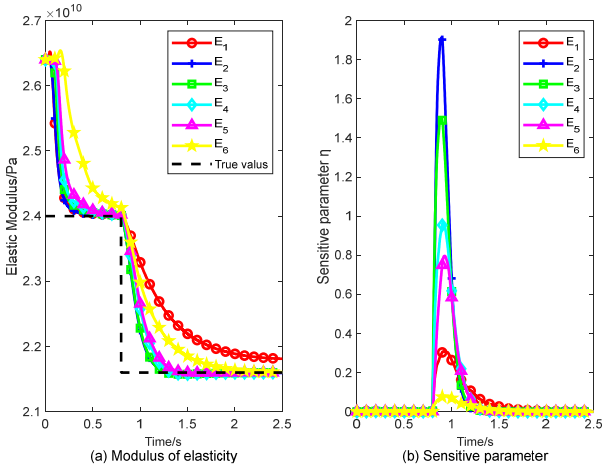

Fig. 5 Comparison of results

Table 1 The true values and calculated initial values of the state vector

State parameters	**u**(m)	**u̇** (ms^{-1})	E_4, E_5 (Nm^{-2})	E_2 (× 10^{10} Nm^{-2})	E_3 (× 10^{10} Nm^{-2})
True values*	$\mathbf{0}_{1\times n}$	$\mathbf{0}_{1\times n}$	2.4 × 10^{10}	$E_2 = \begin{cases} 2.40 & 0 \le t < 0.8 \\ 4.96 - 3.2t & 0.8 \le t < 1.1 \\ 1.44 & 1.1 \le t \le 2.5 \end{cases}$	$E_3 = \begin{cases} 2.40 & 0 \le t < 0.8 \\ 1.56 & 0.8 \le t \le 2.5 \end{cases}$
Initial values of identification	$\mathbf{0}_{1\times n}$	$\mathbf{0}_{1\times n}$	2.64 × 10^{10}	2.64 × 10^{10}	2.64 × 10^{10}

scientific comparison. The specific results can be seen in Fig. 5 and it can be concluded that: (1) the identification results of elastic modulus of beam ① and ⑥ are bad; (2) the variation characteristics of η of beam ① and ⑥ are not obvious; (3) the sensitivity of beam ① and ⑥ to the same observation values are poor.

Because the research on the sensitivity of different observation values does not belong to the scope of this paper. To identify more conveniently, it is assumed that the elastic modulus of ① and ⑥ in Fig. 3 at both ends of the bridge are known in advance. Such operation has no effect on the verification of the proposed adaptive algorithm. Certainly, you can reduce the size of beams ① and ⑥ as much as possible to consider more middle parts.

The specific state vector form is shown in Eq. (26). Since the number of degrees of freedom of the bridge is n = 14 and the number of parameters to be identified is m = 4, then the $(2n + m)$ order vector is taken as the state vector in which the total number of degrees of freedom is 32. The true values and calculated initial values of the state vector are shown in Table 1 where the mixed parameter variation is considered including the abrupt change and gradual change. In the simulation, the values of E_2 and E_3 start to change at 0.8 s. In addition, for the sake of application habits, the identification results are characterized by stiffness which equals EI. The process noise covariance and observation noise covariance matrices are taken as $1 \times 10^{-8}\mathbf{I}$ respectively in the following simulation. The value related to the displacement and velocity in $\mathbf{P}_0$ is taken as 1×10^{-8}, while the value related to the E is taken as 0.01. The five vertical displacements of nodes 2 ~ 6 in Fig. 3 are taken as the observation values and the specific observation equation is as $Y = [y_1 \ y_2 \ y_3 \ y_4 \ y_5]^T = [u_{b4} \ u_{b6} \ u_{b8} \ u_{b10} \ u_{12}]^T$.

$$X(t) = [u_b(t)_{1\times14}\dot{u}_b(t)_{1\times14}\theta_{1\times4}]^T \tag{26}$$

where $\boldsymbol{\theta}$ represents the elastic modulus to be identified, and the dimension is m = 4; '$p \times q$' represents a vector or matrix with p row(s) and q column(s).

$$\dot{X}(t) = \begin{bmatrix} \dot{u}_b(t)_{14\times1} \\ \ddot{u}_b(t)_{14\times1} \\ \dot{\theta}_{4\times1} \end{bmatrix} = \begin{bmatrix} \dot{u}_b(t) \\ M_b^{-1}\left(LF(t) - C_b\dot{u}(t) - K_bu(t)\right) \\ \mathbf{0}_{4\times1} \end{bmatrix} \tag{27}$$

where the quantities appearing in Eq. (27) are defined as $u_b = [u_{b1}, u_{b2}, u_{b3}, \ldots, u_{b14}]^T, \theta = [E_2, E_3, E_4, E_5]^T$

3.2.1 Identifying with low sampling frequency

In the beginning, the sampling frequency (SF) is set to 100 Hz without considering the influence of noise. The specific comparison results are shown in Fig. 6.

As can be seen from Fig. 6, when the structural parameters have time-variant characteristics, the UKF cannot identify the true parameters with SF = 100 Hz, while the AUKF-FF can quickly and accurately converge to the true values, and has a strong parameter tracking ability.

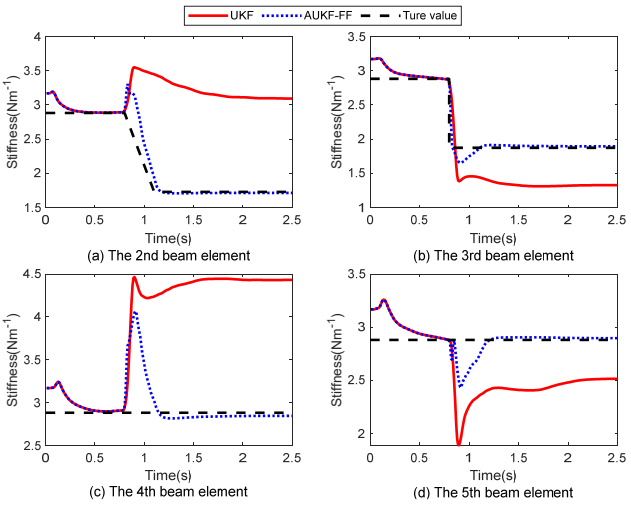

Fig. 6 Stiffness identification results when the noise is 0 (SF = 100 Hz, Stiffness = Y-axis value × 10^9)

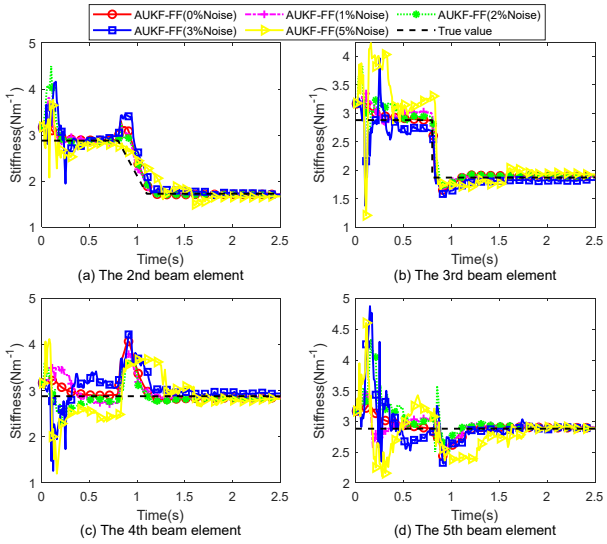

Fig. 7 Stiffness identification results with noise (SF = 100 Hz, Stiffness = Y-axis value × 10^9)

Since the elastic modulus of beam ② and ③ starts to change at 0.8 s, some identification results may generate mutation at this moment (as shown in Figs. 6(c) and (d)).

To explore the robustness of AUKF-FF, the noise which obeys normal distribution is set to 1%, 2%, 3% and 5% successively. The noise over 5% is not considered because the variable characteristics of η will disappear. The identification results are shown in Fig. 7.

As shown in Fig. 7, when the noise is 1%, 2% and 3%, the AUKF-FF can converge to the true values quickly, relatively smoothly and accurately. Even when the noise is up to 5%, it can still track and identify structural parameters successfully although there are some big fluctuations existing.

3.2.2 Identifying with high sampling frequency

Let SF = 1000 Hz and the comparison results with 0 noise are shown in Fig. 8, from which it can be concluded

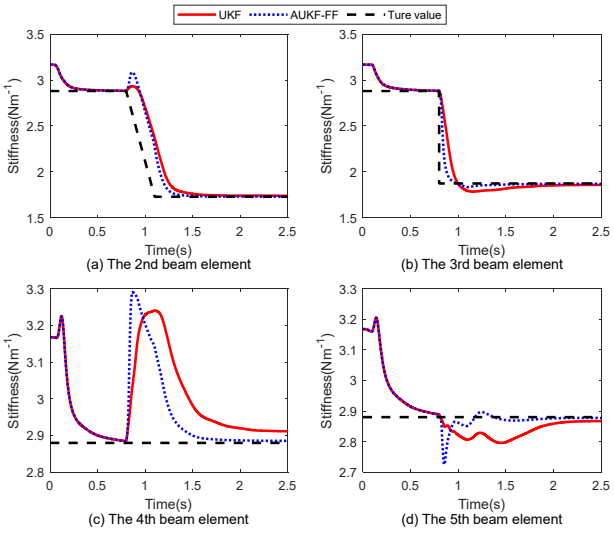

Fig. 8 Stiffness identification results without noise (SF = 1000 Hz, Stiffness = Y-axis value × 10^9)

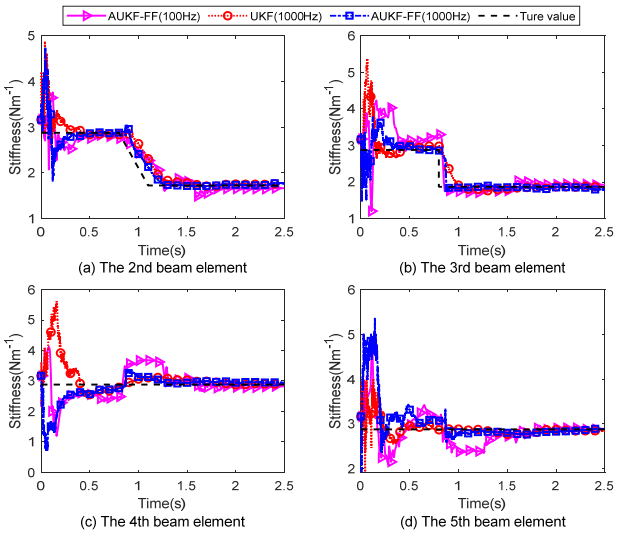

Fig. 9 Stiffness identification results with 5% noise (SF = 1000 Hz, Stiffness = Y-axis value × 10^9)

that the UKF also can acquire the ability to track the time-variant parameters when SF = 1000 Hz, but the AUKF-FF has faster convergence speed and higher convergence accuracy.

To verify the identification effect of the proposed adaptive method under 5% noise when SF = 1000 Hz, here compares three cases: the AUKF-FF algorithm with 100 Hz and 1000 Hz respectively, and the UKF algorithm with 1000 Hz. The specific comparison results are shown in Fig. 9.

As shown in Fig. 9, when SF = 1000 Hz, the robustness of the AUKF-FF algorithm has been improved, and the identification process becomes smoother. Compared with the UKF under 5% noise, the AUKF-FF can better track the time-variant characteristics.

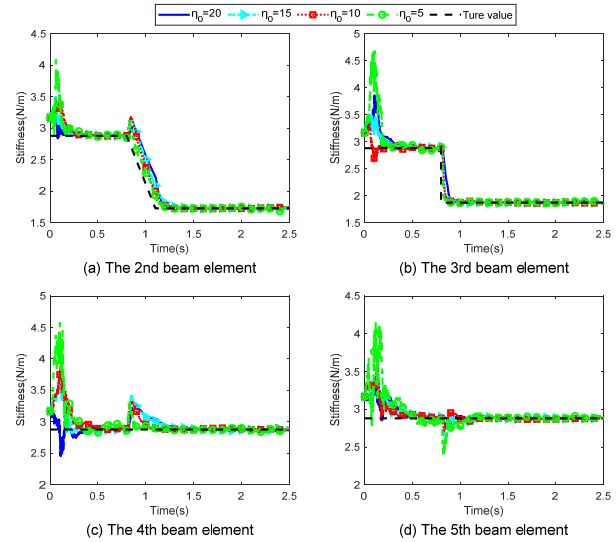

Fig. 10 Stiffness identification results with 1% noise (SF = 1000 Hz, Stiffness = Y-axis value × 10^9)

3.2.3 The effects research of different η_0

When calculating η_0, there still exists a problem of trying. So, it is worthwhile to study the effects of different η_0 on the condition that the identification results are convergent. Based on this idea, take the case of SF = 1000 Hz with 1% noise for example. The comparison results are shown in Fig. 10.

From Fig. 10, it can be found that the smaller the η_0, the more the identification results can reflect the time-variant characteristics of the parameters. And Fig. 10(a) is more obvious. The identification error can be $error_{(\eta 0=5)} < error_{(\eta 0=10)} < error_{(\eta 0=15)} < error_{(\eta 0=20)}$. Besides, the smaller the η_0, the bigger the fluctuation at the initial time and parameter change time. Therefore, given stability and accuracy, we should choose a moderate η_0 value.

3.2.4 Comparison of calculation efficiency

In reality, the earthquake duration is usually transient. To quickly evaluate the structural health status and provide reasonable suggestions for post-disaster decision-making, the calculation efficiency of the program is a key issue. All the results presented in 3.2 were obtained using a laptop computer with Intel(R) Core(TM) i7-6700HQ CPU @ 2.60-GHz processors with 4 cores and 8-GB random-access memory. The specific time consumption is shown in Table 2.

From Table 2, it can be concluded that the time consumption of UKF and AUKF-FF under the same SF is basically equivalent, indicating that the AUKF-FF

Table 2 Calculation time comparison

Algorithm	Sampling frequency (Hz)	Computing time (s)
UKF	100	10.16
AUKF-FF		10.12
UKF	1000	99.19
AUKF-FF		102.57

algorithm does not need additional computing time. Therefore, from a comprehensive comparison, considering timeliness and accuracy, the proposed AUKF-FF algorithm is better than the conventional UKF.

4. Field test validation of adaptive UKF with forgetting factor

4.1 Calculation model simplification

On May 21, 2021, an earthquake of magnitudes 6.4 (M_s 6.4) occurred in Yangbi County, Dali Prefecture, Yunnan Province, China, with a focal depth of 8 km, followed by several aftershocks. The research object, built in 2013, is a six-story concrete frame structure with a building height of 22.95 m and has withstood M_s 4.1, M_s 3.6 and many other small earthquakes successively. After the earthquake, according to the deployment of the China Seismological Bureau, the Institute of engineering mechanics of China Seismological Bureau took the lead in rapidly entering the disaster area to carry out a scientific investigation on the mechanism of strong ground motion and engineering earthquake damage. Fig. 11 are some post-earthquake pictures of the six-story frame structure. According to Fig. 11, the seismic damage is mainly cracked, and no serious seismic damage is found.

Because it is necessary to evaluate the safety of post-earthquake structures, the correct calculation model for in-depth analysis becomes urgent. According to the design drawings, the initial stiffness of each floor can be calculated by the D-value method, and the mass of each floor can also be obtained. See Table 3 for specific parameter values. For the convenience of calculation, the concrete frame structure is simplified into a shear model, and the Rayleigh damping type is adopted, in which the structural damping ratio is set to 0.025 according to the specification. The motion control equation of the structure under earthquake is shown in Eq. (28).

$$M_s\ddot{X}_s + C_s\dot{X}_s + K_sX_s = -M_sL\ddot{X}_g \tag{28}$$

where $\mathbf{M}_s$, $\mathbf{C}_s$ and $\mathbf{K}_s$ are the mass, damping and stiffness matrices of the structure, respectively; $\mathbf{X}_s$, $\dot{X}_s$ and $\ddot{X}_s$ represent the displacement, velocity and acceleration, respectively; $\ddot{X}_g$ stands for the seismic acceleration, and $\mathbf{L}$ is the position vector.

Before model updating, we need to check the effectiveness of the simplified shear model for two purposes: (1) to verify the rationality of the shear model hypothesis; (2) to judge whether the structural parameters change with time. Therefore, we select the acceleration responses, measured by the wireless acceleration sensor during the M_s 3.6 earthquake, as the test data. Since the acceleration values of the 1st, 4th and 6th floors (Fig. 12) were collected during the earthquake. We take the 1st-floor

(a) External wall veneer falling off

(b) Cracks at the bottom of lintel at widow opening

(c) Veneer at the bottom of the column falls off

(d) Vertical cracks in walls

(e) Concrete beam bottom crack

(f) Cross inclined cracks in walls

Fig. 11 Post-earthquake structure

Table 3 The mass and stiffness of each floor of the frame structure

Floor	1st floor	2nd floor	3rd floor	4th floor	5th floor	6th floor
Mass ($\times 10^3$ kg)	404.3	459.1	398.0	366.1	366.1	234.5
Stiffness ($\times 10^6$ Nm^{-1})	80.56	117.99	172.42	172.42	172.42	58.4
Updated Stiffness ($\times 10^6$ Nm^{-1})	80.5598	117.99	172.42	172.42	172.42	58.4354

(a) Front view (b) Side view

Fig. 12 Acceleration sensors arrangement (The red triangle represents the sensor)

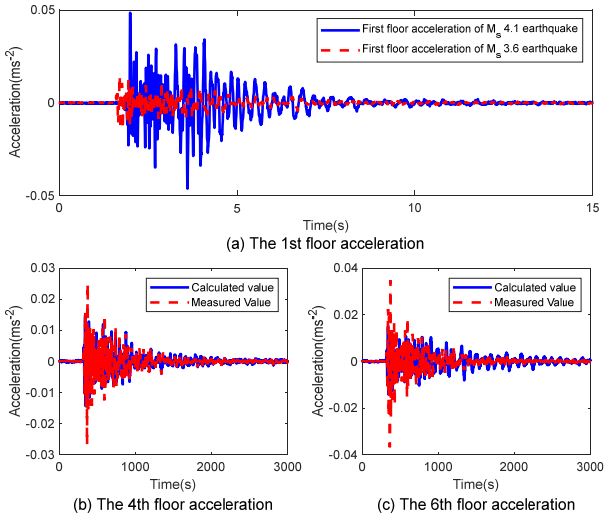

Fig. 13 Seismic excitation input and comparison of acceleration responses

acceleration as the seismic excitation input (Fig. 13(a)) and use the Newmark-β method to calculate the responses of the 4th and 6th floors. The specific comparison results are shown in Fig. 13.

As shown in Fig. 13, the calculated values of the shear model are basically consistent with the measured ones, although there are some small differences existing. The discrepancy may be that the structural parameters has changed during the earthquake interaction. Because the differences are small, it is speculated that the earthquake did little damage to the structure. Generally, it is considered that the structural mass remains unchanged, so it is inferred that the stiffness parameters of the structure need to be fine-tuned and corrected. Although the above results are not the exactly same, it also shows that it is reasonable to simplify the six-story concrete frame structure into a shear model, and what needs to be done is to further optimize the structural parameters.

4.2 Model updating

This part studies the model updating of the six-story concrete frame structure based on the AUKF-FF algorithm and takes the structural stiffness as the parameter to be identified. Since the state vector is mainly composed of the displacement, velocity and stiffness parameters, and the initial displacement and velocity are considered to be zero before the earthquake. In addition, the initial stiffness of the original structure has been calculated through the D-value method. So, the reliability of the initial state information is very high. According to the setting method proposed in Section 2.2, $\mathbf{P}_0$ is set to $1 \times 10^{-6}\mathbf{I}$. As the observed accelerations are actually measured, the observed noise covariance matrix here is set to $1 \times 10^{-8}\mathbf{I}$. Meanwhile, due to the rationality of the shear model, the process noise covariance matrix is also set to $1 \times 10^{-8}\mathbf{I}$.

Because the six-story concrete frame structure has experienced earthquakes of M_s 4.1 and M_s 3.6 successively, and the acceleration responses of the 1st, 4th and 6th floors are collected (Fig. 12), the stiffness parameters are corrected respectively through these two earthquakes, and the stiffness values of the initial state vector in the second identification are equal to the results of the first identification. During identification, the 1st-floor acceleration is taken as the seismic excitation input, as

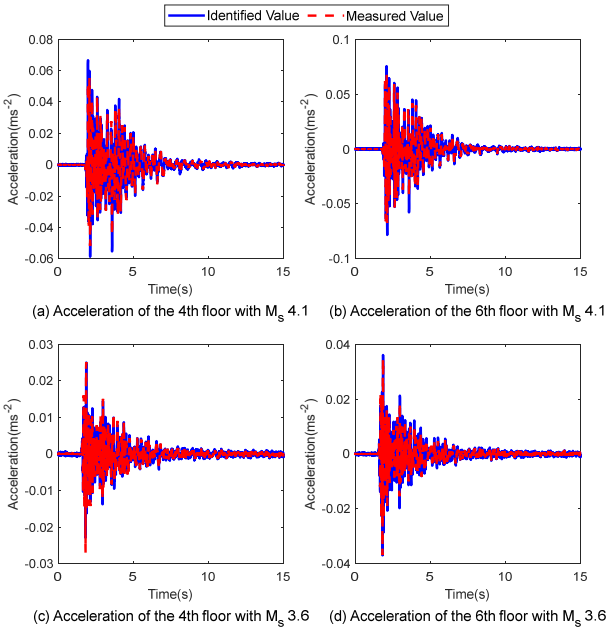

Fig. 14 The comparison of acceleration results

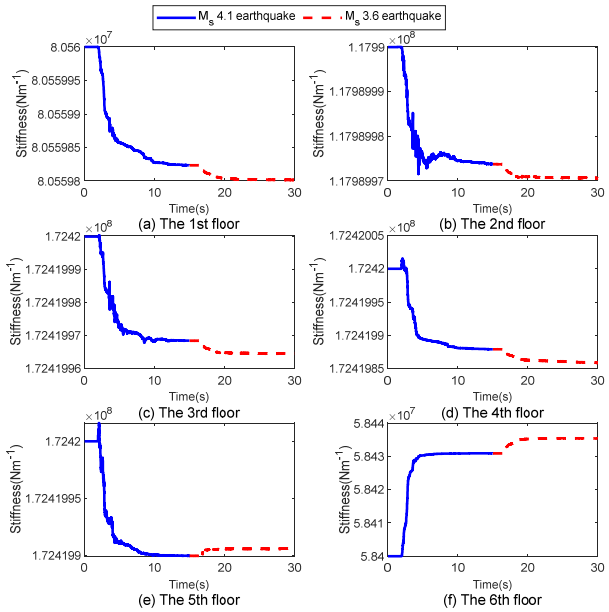

Fig. 15 Stiffness parameter identification results

shown in Fig. 13(a).

The state vector form and state equation of this identification are similar to those of VBS in Section 3.1. For details, please refer to Eqs. (26)~(27). The initial values of the state vector are listed in Table 3, and the accelerations of the 4th and 6th floors are selected as the observed values. The specific comparison of acceleration results is shown in Fig. 14.

As shown in Fig.14, the calculated accelerations of the 4th and 6th floors are in good agreement with the measured ones. It means the identification results are reliable. Besides, the specific parameter identification results are shown in Fig. 15. According to Fig. 15, the stiffness parameters of the frame structure are updated iteratively and tend to be stable after being corrected by AUKF-FF. The final stiffness parameter values after correction are shown in Table 3.

It can be concluded from Table 3 that the stiffness changes of the frame structure are very small. Even after rounding, it is found that the stiffness from the 2nd floor to the 5th floor has not changed at all, which also shows the earthquake did not cause substantial damage to the structure, confirming the speculation in Section 4.1. The conclusion also shows good agreement with what Fig. 11 reflects. In short, the six-story concrete frame structure is safe at present. And after scientific analysis, it provides some theoretical support and kind of technical method for assessing the structural healthy state.

5. Conclusions

Based on the time-variant characteristics of structural parameters under extremely large external excitations, an adaptive UKF with forgetting factor algorithm which can better identify and track the time-variant parameters is proposed in this paper.

- The adaptive algorithm introduces a forgetting factor to modify the state covariance, innovation covariance and cross covariance at the same time, so as to expand the role of new measurement and weaken the cumulative error of previous data.
- Compared with the conventional UKF, it has a faster convergence speed, higher accuracy and better adaptability to a lower sampling frequency.
- The computational efficiency of the adaptive algorithm is basically the same as that of the conventional UKF algorithm, without introducing additional computational power.
- The calculation model updating case of the six-story concrete frame structure under real earthquakes shows that the proposed AUKF-FF method can be applied to practical problems.

Furthermore, due to the small earthquake magnitude considered in this study, the frame structure did not produce substantial damage, thus not involving significant parameter changes. Therefore, the earthquake case in this paper can only verify the safety of the structure, and the ability of AUKF-FF to solve other practical problems will be further studied in the future.

Acknowledgments

The authors gratefully acknowledge the financial support by the National Key R&D Program of China [Grant No. 2021YFB2600605, 2021YFB2600600], the Key R&D Program of Hebei Province [Grant No. 19275405D], the Hebei Provincial Transport Bureau Research Program [Grant No. TH-201902] and Scientific Research Fund of Institute of Engineering Mechanics, China Earthquake Administration [Grant No. 2019D22].

References

Ahmed-Ali, T., Kenne, G. and Lamnabhi-Lagarrigue, F. (2009), "Identification of nonlinear systems with time-varying parameters using a sliding-neural network observer", *Neurocomputing*, **72**, 1611-1620. https://doi.org/10.1016/j.neucom.2008.09.001

Asl, R.M., Hagh, Y.S., Simani, S. and Handroos, H. (2019), "Adaptive square-root unscented Kalman filter: An experimental study of hydraulic actuator state estimation", *Mech. Syst. Signal Process.*, **132**, 670-691. https://doi.org/10.1016/j.ymssp.2019.07.021

Astroza, R., Ebrahimian, H. and Conte, J. (2019a), "Performance comparison of Kalman−based filters for nonlinear structural finite element model updating", *J. Sound Vib.*, **438**, 520-542. https://doi.org/10.1016/J.JSV.2018.09.023

Astroza, R., Alessandri, A. and Conte, J.P. (2019b), "A dual adaptive filtering approach for nonlinear finite element model updating accounting for modeling uncertainty", *Mech. Syst. Signal Process.*, **115**, 782-800. https://doi.org/10.1016/j.ymssp.2018.06.014

Bao, Y., Velni, J.M., Basina, A. and Shahbakhti, M. (2020), "Identification of state-space linear parameter-varying models using artificial neural networks", *IFAC-PapersOnLine*, **53**,

5286-5291. https://doi.org/10.1016/J.IFACOL.2020.12.1209
Bisht, S.S. and Singh, M.P. (2014), "An adaptive unscented Kalman filter for tracking sudden stiffness changes", *Mech. Syst. Signal Process.*, **49**, 181-195. https://doi.org/10.1016/j.ymssp.2014.04.009
Calabrese, A., Strano, S. and Terzo, M. (2018), "Adaptive constrained unscented Kalman filtering for real-time nonlinear structural system identification", *Struct. Control Health Monitor.*, **25**. https://doi.org/10.1002/STC.2084
Cao, J.X., Xiong, H.B. and Chen, L. (2020), "Procedure for parameter identification and mechanical properties assessment of CLT connections", *Eng. Struct.*, **203**. https://doi.org/10.1016/j.engstruct.2019.109867
Chen, Y.Y. and Zhou, Y.W. (2020), "Machine learning based decision making for time varying systems: parameter estimation and performance optimization", *Knowl. Based Syst.*, **190**. https://doi.org/10.1016/j.knosys.2020.105479
Chin, R., Maass, A.I., Ulapane, N., Manzie, C., Shames, I., Nešić, D., Rowe, J.E. and Nakada, H. (2020), "Active learning for linear parameter-varying system identification", ArXiv, abs/2005.00711. https://doi.org/10.1016/J.IFACOL.2020.12.1274
Chowdhary, G. and Jategaonkar, R. (2010), "Aerodynamic parameter estimation from flight data applying extended and unscented Kalman filter", *Aerosp. Sci. Technol.*, **14**(2), 106-117. https://doi.org/10.1016/j.ast.2009.10.003
Chung, M.J. and Sato, T. (2006), "Structural identification using stochastic filtering techniques based on measurements from wireless data acquisition system", *Steel Struct.*, **6**, 353-360.
Cui, M., Khodayar, M., Chen, C., Wang, X., Zhang, Y. and Khodayar, M.E. (2019), "Deep learning based time-varying parameter identification for system-wide load modeling", *LEEE Transact. Smart Grid*, **10**, 6102-6114. https://doi.org/10.1109/Tsg.2019.2896493
Ding, Y., Guo, L.N. and Zhao, B. (2017), "Parameter Identification for Nonlinear Structures by a Constrained Kalman Filter with Limited Input Information", *Int. J. Struct. Stabil. Dyn.*, **17**, 1750010. https://doi.org/10.1142/S0219455417500109
Doebling, S.W., Farrar, C.R. and Prime, M.B. (1998), "A summary review of vibration-based damage identification methods", *Shock Vib. Digest*, **30**(2), 91-105. https://doi.org/10.1177/058310249803000201
Guo, L.N., Ding, Y., Wang, Z., Xu, G.S. and Wu, B. (2018), "A dynamic load estimation method for nonlinear structures with unscented Kalman filter", *Mech. Syst. Signal Process.*, **101**, 254-273. https://doi.org/10.1016/j.ymssp.2017.07.047
Hu, P.D., Zhang, M.Z., Zhang, R., Wu, Q.P. and Yang, A.L. (2021), "Correlation method and Kalman filter-based adaptive angle rate estimation for time-varying periodic signals of the attitude and heading reference system", *Mech Syst. Signal Process.*, **156**. https://doi.org/10.1016/j.ymssp.2021.107695
Humar, J., Bagchi, A. and Xu, H.P. (2006), "Performance of vibration-based techniques for the identification of structural damage", *Struct. Health Monitor.*, **5**, 215-241. https://doi.org/10.1177/1475921706067738
Jategaonkar, R. and Plaetenschke, E. (1998), "Estimation of aircraft parameters using filter error methods and extended Kalman filter", DFVLR FB, 88-15.
Julier, S.J., Uhlmann, J.K. and Durrant-Whyte, H.F. (1995), "A new approach for filtering nonlinear systems", *Proceedings of 1995 American Control Conference-ACC'95*, **3**, 1628-1632. https://doi.org/10.1109/ACC.1995.529783
Manoach, E., Samborski, S., Mitura, A. and Warminski, J. (2012), "Vibration based damage detection in composite beams under temperature variations using Poincaré maps", *Int. J. Mech. Sci.*, **62**, 120-132. https://doi.org/10.1016/J.IJMECSCI.2012.06.006
Mariani, S. and Ghisi, A. (2007), "Unscented Kalman filtering for nonlinear structural dynamics", *Nonlinear Dyn.*, **49**, 131-150. https://doi.org/10.1007/s11071-006-9118-9
Masti, D., Bernardini, D. and Bemporada, A. (2021), "A machine-learning approach to synthesize virtual sensors for parameter-varying systems", ArXiv, 61, 40-49. https://doi.org/10.1016/j.ejcon.2021.06.005
Mulay, A., Ben, B.S., Ismail, S. and Kocanda, A. (2019), "Prediction of average surface roughness and formability in single point incremental forming using artificial neural network", *Arch. Civil Mech. Eng.*, **19**, 1135-1149. https://doi.org/10.1016/j.acme.2019.06.004
Naranjo-Pérez, J., Jiméneš Alonso, J.F., Pavic, A. and Sáez, A. (2020), "Finite-element-model updating of civil engineering structures using a hybrid UKF-HS algorith", *Struct. Infrastr. Eng.*, **17**, 620-637. https://doi.org/10.1080/15732479.2020.1760317
Nguyen, H., Vu, T., Vo, T.P. and Thai, H.T. (2021), "Efficient machine learning models for prediction of concrete strengths", *Constr. Build. Mater.*, **266**. https://doi.org/10.1016/j.conbuildmat.2020.120950
Pappalardo, C.M. and Guida, D. (2016), "Control of nonlinear vibrations using the adjoint method", *Meccanica*, **52**, 2503-2526. https://doi.org/10.1007/s11012-016-0601-1
Pappalardo, C.M. and Guida, D. (2017), "Adjoint-Based Optimization Procedure for Active Vibration Control of Nonlinear Mechanical Systems", *J. Dyn. Syst. Measure. Control-Transact. ASME*, **139**, 081010. https://doi.org/10.1115/1.4035609
Rahimi, A., Kumar, K.D. and Alighanbari, H. (2017), "Fault estimation of satellite reaction wheels using covariance based adaptive unscented Kalman filter", *Acta Astronautica*, **134**, 159-169. https://doi.org/10.1016/j.actaastro.2017.02.003
Sadhukhan, C., Mitra, S.K., Naskar, M.K. and Sharifpur, M. (2021), "Fault diagnosis of a nonlinear hybrid system using adaptive unscented Kalman flter bank", *Eng. Comput.*, **38**, 2717-2728. https://doi.org/10.1007/s00366-020-01235-0
Schleiter, S. and Altay, O. (2020), "Identification of abrupt stiffness changes of structures with tuned mass dampers under sudden events", *Struct. Control Health Monitor.*, **27**. https://doi.org/10.1002/stc.2530
Shu, X.S., Bao, T.F., Li, Y.T., Gong, J. and Zhang, K. (2021), "VAE-TALSTM: a temporal attention and variational autoencoder-based long short-term memory framework for dam displacement prediction", *Eng. Comput.* https://doi.org/10.1007/s00366-021-01362-2
Song, M., Astroza, R., Ebrahimian, H., Moaveni, B. and Papadimitriou, C. (2020), "Adaptive Kalman filters for nonlinear finite element model updating", *Mech. Syst. Signal Process.*, **143**. https://doi.org/10.1016/j.ymssp.2020.106837
Soyoz, S. and Feng, M.Q. (2009), "Long-term monitoring and identification of bridge structural parameters", *Comput.-Aided Civil Infrastr. Eng.*, **24**, 82-92. https://doi.org/10.1111/j.1467-8667.2008.00572.x
Taffese, W.Z. and Sistonen, E. (2017), "Machine learning for durability and service-life assessment of reinforced concrete structures: Recent advances and future directions", *Automat. Constr.*, **77**, 1-14. https://doi.org/10.1016/j.autcon.2017.01.016
Wang, L.J., Xie, Y.X., Wu, Z.J., Du, Y.X. and He, K.D. (2018), "A new fast convergent iteration regularization method", *Eng. Comput.*, **35**, 127-138. https://doi.org/10.1007/s00366-018-0588-4
Wang, N., Li, L.Y. and Wang, Q. (2019), "Adaptive UKF-Based Parameter Estimation for Bouc-Wen Model of Magnetorheological Elastomer Materials", *J. Aerosp. Eng.*, **32**, https://doi.org/10.1061/(ASCE)AS.1943-5525.0000961-4
Xiao, X., Xu, X. and Shen, W. (2020), "Simultaneous identification of the frequencies and track irregularities of high-

speed railway bridges from vehicle vibration data", *Mech*. *Syst*. *Signal Process*., **152**, 107412. https://doi.org/10.1016/j.ymssp.2020.107412

Yan, G., Sun, H. and Büyüköztürk, O. (2016), "Impact load identification for composite structures using Bayesian regularization and unscented Kalman filter", *Struct*. *Control Health Monitor*., **24**(5). https://doi.org/10.1002/stc.1910

Yang, J.N. and Lin, S. (2005), "Identification of parametric variations of structures based on least squares estimation and adaptive tracking technique", *J*. *Eng*. *Mech*., **131**, 290-298. https://doi.org/10.1061/(Asc(e)0733-9399(2005)131:3(290)

Yang, J.N., Lin, S.L., Huang, H.W. and Zhou, L. (2006), "An adaptive extended Kalman filter for structural damage identification", *Struct*. *Control Health Monitor*., **13**, 849-867. https://doi.org/10.1002/stc.84

Zhou, W., Li, X.L., Yi, J. and He, H.B. (2019), "A Novel UKF-RBF Method based on adaptive noise factor for fault diagnosis in pumping unit", *IEEE Transact*. *Indust*. *Inform*., **15**. https://doi.org/1415-1424. 10.1109/TII.2018.2839062

HJ